The Second Intracellular Loop of the Calcitonin Gene-related Peptide Receptor Provides Molecular Determinants for Signal Transduction and Cell Surface Expression*

Alex C. Conner[‡§], **John Simms**[‡], **Stephen G. Howitt**[‡], **Mark Wheatley**[§], and **David R. Poyner**[‡1]

From the ‡*School of Life and Health Sciences, Aston University, Birmingham B4 7ET and the* §*School of Biosciences, University of Birmingham, Birmingham B15 2TT, United Kingdom*

The calcitonin gene-related peptide (CGRP) receptor is a heterodimer of a family B G-protein-coupled receptor, calcitonin receptor-like receptor (CLR), and the accessory protein receptor activity modifying protein 1. It couples to G_s, but it is not known which intracellular loops mediate this. We have identified the boundaries of this loop based on the relative position and length of the juxtamembrane transmembrane regions 3 and 4. The loop has been analyzed by systematic mutagenesis of all residues to alanine, measuring cAMP accumulation, CGRP affinity, and receptor expression. Unlike rhodopsin, ICL2 of the CGRP receptor plays a part in the conformational switch after agonist interaction. His-216 and Lys-227 were essential for a functional CGRP-induced cAMP response. The effect of (H216A)CLR is due to a disruption to the cell surface transport or surface stability of the mutant receptor. In contrast, (K227A)CLR had wild-type expression and agonist affinity, suggesting a direct disruption to the downstream signal transduction mechanism of the CGRP receptor. Modeling suggests that the loop undergoes a significant shift in position during receptor activation, exposing a potential G-protein binding pocket. Lys-227 changes position to point into the pocket, potentially allowing it to interact with bound G-proteins. His-216 occupies a position similar to that of Tyr-136 in bovine rhodopsin, part of the DRY motif of the latter receptor. This is the first comprehensive analysis of an entire intracellular loop within the calcitonin family of G-protein-coupled receptor. These data help to define the structural and functional characteristics of the CGRP-receptor and of family B G-protein-coupled receptors in general.

G-Protein coupled receptors (GPCRs)[2] comprise a large superfamily of membrane-spanning proteins encoded by 2–3% of the human genome. These receptors respond to an incredibly diverse array of stimuli from odorants, amines, peptides, and light through a series of broadly similar activation mechanisms and accessory proteins. The pharmaceutical implications of understanding these proteins cannot be underestimated, and the crystal structure of rhodopsin has presented many new avenues of study for this family (1).

Several structural and functional motifs are well characterized within the intracellular domains of the largest known family (A) of GPCRs. These include the conserved (D/E)R(Y/H) motif on the boundary between transmembrane helix 3 and the second intracellular loop (ICL2) and which is well documented to have a significant role in the activation mechanism (2) and the NP*XX*Y motif of TM7, which can have diverse roles in the constitutive phosphorylation, internalization, and signaling of many family A GPCRs (3, 4). In addition, residues within ICL2 juxtaposed to transmembrane helix 3 have been shown to be involved in receptor stability (5).

In contrast, much less is known about the important amino acids of family B receptors, which include the calcitonin family of receptors and which tend to bind larger peptide agonists. There are no obvious common motifs between family A and family B receptors; nevertheless, a shared mechanism involving a ligand-induced conformational distortion between the distal regions of TMs 3 and 6 has been proposed for the parathyroid hormone receptor (6) and the CGRP/adrenomedullin receptors (7). There are contrary reports arguing for the involvement of the second intracellular loop in receptor expression and activation within the family B GPCRs. A recent study on the VPAC1 receptor found that all residues of ICL2 could be mutated without alteration of receptor expression or adenylyl cyclase response to vasoactive intestinal peptide (8). Conversely, a lysine residue in ICL2 of the parathyroid hormone (PTH) receptor was shown to be critical in activating the phospholipase C pathway while having no effect on the adenylyl cyclase response (9).

The family B receptor CLR is unusual among GPCRs in that it requires the co-expression of one of a family of accessory proteins called RAMPs (receptor activity modifying proteins) for cell trafficking and ligand interaction (10). A functional CGRP receptor is formed by a CLR/RAMP1 heterodimer (11). In addition, an agonist-mediated signaling response requires the co-localization of a third membrane-associated accessory protein called the receptor component protein (12). Receptor component protein is thought to form an ionic interaction with the membrane adjacent to CLR (13). There are no studies exploring the role of intracellular regions of CLR involved in CGRP binding, cAMP signaling, or protein expression; indeed there are very few mutational analyses of the second intracellular loop for any family B GPCRs.

This report describes the systematic substitution of all residues of ICL2 of human CLR. Mutations were constructed either individually or in pairs replacing the side chains with a single methyl group (alanine). The naturally occurring alanine residues at position 221 and 224 were replaced with glycine. These mutants were transfected into mammalian cells in combination with a RAMP1 construct and analyzed using a tritiated cAMP radio receptor assay. The assay compared the CGRP-stimulated cAMP accumulation of mutant with wild-type CLR. Mutants with impaired function were further characterized for cellular

[1] To whom correspondence should be addressed. Tel.: 44-121-204-3997; Fax: 44-121-359-5142; E-mail: D.R.Poyner@aston.ac.uk.

[2] The abbreviations used are: GPCR, G-protein coupled receptor; TM, transmembrane helix; ICL, intracellular loop; HA, hemagglutinin; BSA, bovine serum albumin; TBS, Tris-buffered saline; ELISA, enzyme-linked immunosorbant assay; PBS, phosphate-buffered saline; MD, molecular dynamics; WT, wild type; RAMP, receptor activity modifying protein; CLR, calcitonin receptor-like receptor; CGRP, calcitonin gene-related peptide.

expression, ligand affinity, and surface localization. We identify His-216 and Lys-227 as key residues for normal receptor function and utilize molecular modeling to reveal the likely spatial positioning of the second intracellular loop in the predicted active and inactive states of the receptor. Our findings are discussed in the context of previously proposed motifs within this region in other family B receptors.

EXPERIMENTAL PROCEDURES

Materials—Human αCGRP was from Calbiochem. Peptides were dissolved in distilled water and stored as aliquots at -20 °C in non-stick microcentrifuge tubes (Thermo Life Sciences, Basingstoke, UK). Unless otherwise specified, chemicals were from Sigma or Fisher. Cell culture reagents were from Invitrogen or Sigma. [^{125}I]Iodohistidyl[8]-human αCGRP (2000 Ci/mmol) was from Amersham Biosciences.

Expression Constructs and Mutagenesis—Human CLR with an N-terminal hemagglutinin (HA) epitope tag (YPYDVPDYA) (14) was provided by Dr. S. M. Foord (GlaxoSmithKline) and was subcloned into pcDNA3($-$) (Invitrogen) before mutagenesis. Introduction of the epitope did not affect the pharmacology of the receptor (14).

Mutagenesis was carried out using the QuikChange site-directed mutagensis kit (Stratagene, Cambridge, UK), following the manufacturer's instructions. Forward and reverse oligonucleotide primers were designed with single base changes to incorporate amino acid point mutations alanine (or glycine) in the final CL protein and to engineer restriction sites to aid screening of mutants. The primers were synthesized by Invitrogen. The numbering of the residues accommodates a 22-amino acid signal protein before the start of the mature transcript (15).

Plasmid DNA was extracted from the cultures using a Wizard-Prep DNA extraction kit according to the manufacturer's instructions (Promega, Southampton, UK). The plasmid DNA was eluted in 100 μl of sterile distilled water and stored at -20 °C. Sequences were confirmed by sequencing (Functional Genomics, Birmingham, UK).

Cell Culture and Transfection—Cos-7 cells were cultured in Dulbecco's modified Eagle's medium supplemented with 10% (v/v) fetal bovine serum and 5% (v/v) penicillin/streptomycin in a humidified 95% air, 5% CO_2 atmosphere. For transfection, the cells were plated onto either 12- and 48-well plates or 100-mm dishes. Cells were transfected using a mixture (per 1 μg of DNA) of 6 μl of 10 mM polyethyleneimine and 45 μl of 5% glucose solution incubated for 30 min at room temperature and added to an appropriate final volume of full media. 12- and 48-well plates were treated with 1 μg of DNA/well, and 100-mm dishes were treated with 10 μg of DNA/dish. Characterization of expressed receptors was performed 48–72 h after transfection.

Membrane Preparation—The cells from each 100-mm plate were washed briefly with 1 ml of cold phosphate-buffered saline and scraped into a small volume of buffer (20 mM HEPES, 2 mM $MgCl_2$, 1% (w/v) bovine serum albumin (BSA), pH 7.5). The cells were homogenized using an Ultra Turrax homogenizer (full speed for 20 s). The cells were then centrifuged at 20,000 $\times$ g for 30 min at 4 °C. The supernatant was removed, and the pellets were resuspended in 14 ml of buffer (as before) and used immediately for binding studies or stored at -70 °C.

Radioligand Binding—Membranes were homogenized briefly before use, and 500 μl were incubated with 100 pM [^{125}I]iodohistidyl[8]-human αCGRP and appropriate dilutions of human αCGRP for 60 min at room temperature. Nonspecific binding was measured in the presence of 1 μM CGRP. The samples were then centrifuged at 12,000 $\times$ g in a bench-top microcentrifuge for 5 min at room temperature. The pellets were washed twice with water, and the radioactivity was counted in a γ counter.

Assay of cAMP Production—Growth medium was removed from the cells and replaced with Dulbecco's modified Eagle's medium containing 500 μM isobutylmethylxanthine for 30 min. αCGRP in the range 10 pM to 1 μM was added for a further 15 min. Ice-cold ethanol (95–100% v/v) was used to extract cAMP, which was subsequently measured by radio-receptor assay as previously described (16)

Analysis of Cell-surface Expression of Mutants by Enzyme-linked Immunosorbant Assay (ELISA)—Cells in 12-well plates were transiently transfected with wild type (WT) or mutant HA epitope-tagged human CL and RAMP 1. The transfected cells were treated with 3.7% formaldehyde for 15 min after aspiration of growth medium. The cells were then washed 3 times with 0.5 ml of Tris-buffered saline (TBS). Nonspecific binding of the antibody was blocked with 1% BSA in TBS for 45 min. The cells were treated with 250 μl of primary antibody (mouse, anti-HA antibody 12CA5 (Sigma) diluted 1:1000 in TBS with 1% BSA) for 1 h, and the cells were washed again 3 times with 0.5 ml of TBS. A further block step was performed for 15 min before the cells were incubated with 250 μl of secondary antibody (anti-mouse, horseradish peroxidase-conjugated (Sigma) diluted 1:1000 in TBS) for 1 h. The cells were washed a further three times before development with *O*-phenylenediamine tablets (Bio-Rad) according to the manufacturer's instructions. Reactions were terminated with 100 μl/well of 1 M H_2SO_4. The absorbance measured by the ELISA showed a linear dependence on the DNA concentration used in the transfection.

Immunohistocytochemistry—Cos-7 cells were seeded in 6-well plates containing nitric acid-washed glass coverslips (12 mm) and transfected using polyethyleneimine as described above. Cells were fixed and washed with phosphate-buffered saline (PBS) as described previously for the ELISA. Cells were blocked with 1% BSA in PBS for 45 min followed by incubation with an anti-HA primary antibody (diluted to 1:3000 in 3% (w/v) for 60 min. Cells were washed 3 times with PBS before reblocking with 1% BSA in PBS for 15 min at room temperature. Cells were labeled with a staining mixture including goat anti-mouse IgG conjugated to fluorescein isothiocyanate (Sigma) (diluted to 1:500 in 10% (v/v) goat serum in PBS), Alexa 546 phalloidin (Molecular Probes, Leiden, The Netherlands), and Hoescht 33342 (Sigma) for 60 min at room temperature in the dark. After a further three washes, coverslips were mounted on glass slides before confocal microscopy.

Confocal Microscopy—Confocal microscopy was performed using a Nikon Optiphat II laser scanning microscope at 60$\times$ magnification under immersion oil. The HA-tagged receptors were visualized by exciting the secondary antibody, actin filaments were visualized by exciting the Alexa 546 phalloidin, and nuclei were visualized by exciting the Hoescht 33342. The appropriate wavelength was used according to manufacturer's instructions in each case. Images were captured at 10 random sites for each slide from three separate experiments.

TM Prediction—Individual TM helix prediction of 58 diverse Family B GPCR sequences was performed using the web-based versions of TMHMM2 (17) and HMMTOP2 (18). A consensus prediction for the boundaries of TMIII and TMIV was generated by visual inspection, and from this initial survey, a ClustalW (19) profile alignment (using the Blosum matrix) was created against 58 peptide hormone family A GPCRs. The resulting alignment was used to generate an initial homology based model using the high resolution x-ray crystal structure of bovine rhodopsin as a template. Further refinement of the homology model was achieved through molecular dynamics (MD) simulations of the receptor embedded in a dipalmitoylphosphatidylcholine bilayer. A series ($n = 5$) of 5-ns MD simulations were carried out using the GROMOS96 force field parameter set, with minor modifications, as implemented in GROMACS (20). The resulting trajectories were concate-

TABLE 1

Conservation of residues within ICL2 of CLR

ICL2 boundaries are assumed from the model presented in this study. The table compares CLR with 57 diverse GPCR examples from family B taken from www.expasy.ch.

CLR	% Identity	CLR	% Identity	CLR	% Identity
Tyr-214	100	Val-221	15	Gln-228	18
Leu-215	100	Ala-222	27	His-229	19
His-216	56	Val-223	21	Leu-230	34
Thr-217	47	Phe-224	42	Met-231	26
Leu-218	71	Ala-225	29	Trp-232	19
Ile-219	48	Glu-226	50	Tyr-233	45
Val-220	36	Lys-227	28		

nated and used to produce the final refined model of the CLR. The active state of the CLR was achieved through the use of a modified rhodopsin template, which was consistent with experimentally derived distance restraints obtained from the literature (21–25). Homology models of the active CLR were refined through the use of MD simulations as described above.

Prediction of the ICL2 of Rhodopsin and the CLR—RAPPER was used to predict from first principles (*ab initio*) the conformations of ICL2 from rhodopsin and the CLR. Briefly, 1000 loop backbone conformations were generated using RAPPER assuming idealized stereochemistry for all heavy atoms (N, Cα, C, O). The side-chain orientations for the predicted backbone conformations were modeled using SCWRL (26) within the environment of the remaining, non-modeled protein. Generated fragments were initially scored using an all-atom statistical potential (scop-e4-allatoms-x-ray-scores scoring set) as described by Samudrala and Moult (27). The ensemble of loop conformations was filtered on the basis of a RADPF score such that no more than the top 50 models were retained for energy minimization. Minimization was performed using a l-BFGS minimization method which utilized the AMBER all-atom force-field (parm99) together with the Still GB/SA solvation model, as implemented in the TINKER (28). Minimization was performed until either convergence or a 0.1-kcal mol^{-1} cutoff point was reached. Only atoms belonging to either the loop region or the N/C-terminal anchor residues were allowed to move during minimization. Minimized fragments were subsequently ranked according to the conformational free energy of the loop.

Data Analysis—Curve fitting was done with PRISM Graphpad 4 (Graphpad Software Inc., San Diego, CA). For cAMP studies, the data from each concentration-response curve were fitted to a sigmoidal concentration-response curve to obtain the maximum response and $-\log EC_{50}$ (pEC_{50}). For radioligand binding experiments curves were fitted to obtain maximum and minimum amounts of binding and $-\log IC_{50}$ (pIC_{50}). Because the radioligand was present at concentrations well below its K_d, the IC_{50} values were effectively identical to the K_i values. To estimate B_{max} values with ^{125}I-labeled CGRP, the data were fitted to a sigmoidal curve, calculating the amount bound from the specific activity of the radioligand (this was progressively reduced by dilution with unlabeled CGRP). pEC_{50}, pIC_{50}, and B_{max} values were compared by paired Student's t test. Comparisons were only made between wild-type (WT) and mutant data from concomitantly transfected cells. A control WT experiment was always performed alongside a mutant experiment.

RESULTS

Identification of the Boundaries of ICL2—According to the Swiss-Prot data base entry Q16602 (www.ExPasy.org), ICL2 of the CLR would be predicted to encompass residues from (and including) Leu-215 to Met-230. An alignment of this region of 57 family B GPCRs in Table 1 shows the most conserved amino acids. The TM/loop boundaries were more precisely defined by using a consensus of previously validated TM
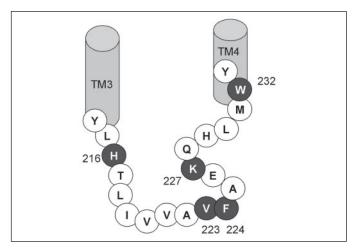

FIGURE 1. Amino acid sequence of ICL2 from human CL showing the positions of the mutated residues. Residues in *black* showed reductions in the CGRP-stimulated adenylate cyclase activation in this study. Residue numbering is from the start of the predicted mature transcript of CLR (15).

prediction methods and remote sequence alignment to a known structure. Visual inspection of the TM prediction results revealed that, although the boundaries for TM4 were well defined, those for TM3 exhibited variability. Essentially, the predicted boundaries for TM3 were clustered into two populations. The first population, which included the majority of sequences studied (40 of 58), exhibited a TM3 boundary at the equivalent position to residues 214 and 243 (including the signal peptide) of the CLR. Significantly, this would position the conserved cysteine residue located at the extracellular end of TM3 in the same positions as that observed in family A receptors. The boundaries for TM3 of the second, smaller population was between the equivalent residues to 227 and 247 (CLR). We have, therefore, used the boundaries exhibited by the first, larger population for subsequent loop modeling studies. As previously mentioned, the predicted boundaries for TM4 were well defined and included residues 250–270 (CLR). Furthermore, sequence alignment of the predicted TM4 segment against the residues corresponding to the high resolution x-ray crystal structure of rhodopsin positioned a conserved tryptophan residue found in both family A and B GPCRs in the same position.

Effect of ICL2 Substitution Mutants on cAMP Accumulation—To identify the contribution to CGRP-stimulated signaling provided by residues within this ICL2 and adjoining segments, residues between Tyr-214 and Tyr-233 inclusive (see Fig. 1) were mutated to alanine either individually or in pairs to generate the constructs (Y214A/L215A)CLR, (H216A)CLR, (T217A)CLR, (L218A/I219A)CLR, (V220A/V221A)-CLR, (A222G)CLR, (V223A/F224A)CLR, (A225G)CLR, (E226A)CLR, (K227A)CLR, (Q228A/H229A)CLR, (L230A/M231A)CLR, (W232A)-CLR, and (Y233A)CLR. Each mutant receptor construct was co-expressed with a RAMP1 vector in Cos-7 cells, and the CGRP-stimulated cAMP accumulation was compared with wild-type CLR. In each
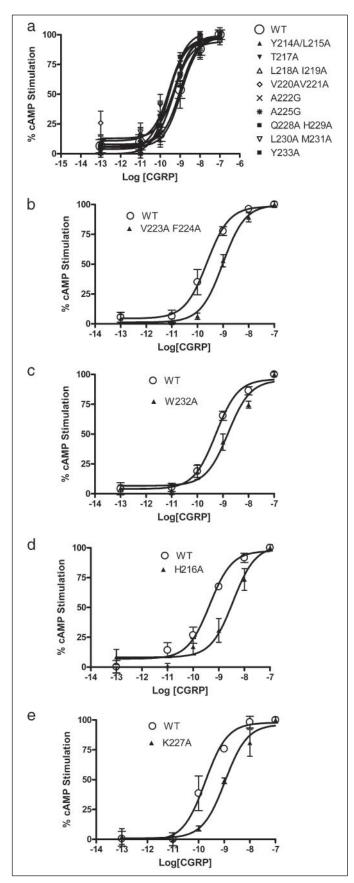
FIGURE 2. **CGRP-stimulated cAMP response of the ICL2 mutants.** Cos-7 cells were transfected with WT/RAMP1 or mutant/RAMP1 and assayed for CGRP-stimulated cAMP production. *Open circles*, WT type receptors. Mutant receptors are as indicated. Data are

TABLE 2

Functional parameters of WT/RAMP1 and mutant receptors

Values are the mean $\pm$ S.E; the number of determinations is shown in parentheses. The maximum responses (E_{max}) were not significantly different from the concomitantly expressed WT receptor for all of the mutants in this study (data not shown).

Mutant	WT pEC$_{50}$	pEC$_{50}$
(Y214A/L215A)CLR	9.02 ± 0.21 (3)	8.91 ± 0.36 (3)
(H216A)CLR	9.41 ± 0.13 (3)	8.37 ± 0.37(3)[a]
(T217A)CLR	9.36 ± 0.21 (3)	9.33 ± 0.35 (3)
(L218A/I219A)CLR	9.66 ± 1.01 (3)	9.37 ± 1.04 (3)
(V220/V221A)CLR	9.75 ± 0.36 (3)	9.64 ± 0.11 (3)
(A222G)CLR	9.54 ± 0.12 (3)	9.54 ± 0.34 (3)
(V223A/F224A)CLR	9.62 ± 0.05 (3)	9.02 ± 0.13(3)[b]
(A225G)CLR	9.43 ± 0.21 (3)	9.34 ± 0.19 (3)
(E226A)CLR	10.07 ± 0.09 (3)	9.87 ± 0.20 (3)
(K227A)CLR	9.97 ± 0.37 (3)	8.91 ± 0.23(3)[a]
(Q228A/H229A)CLR	9.60 ± 0.75 (3)	9.55 ± 0.52 (3)
(L230A/M231A)CLR	9.44 ± 0.21 (3)	9.65 ± 0.39 (3)
(W232A)CLR	9.27 ± 0.10 (3)	8.85 ± 0.32(3)[b]
(Y233A)CLR	8.84 ± 0.06 (3)	8.50 ± 0.10 (3)

[a] Significantly different from WT, $p < 0.01$, as assessed by paired Student's t test.
[b] Significantly different from WT, $p < 0.05$, as assessed by paired Student's t-test.

case during this study, the natural α-CGRP agonist was used to generate dose response curves.

As shown in Fig. 2*a* and Table 2, the pEC$_{50}$ for cAMP production in response to CGRP was not significantly different for the seven alanine substitution mutants (Y214A/L215A)CLR, (T217A)CLR, (L218A/I219A)CLR, (V220A/V221A)CLR, (Q228A/H229A)CLR, (L230A/M231A)CLR, and (Y233A)CLR or the two glycine substitution mutants (A222G)CLR and (A225G)CLR when compared with WT CLR co-transfected with RAMP1. Additionally, none of the point mutations in this study had basal levels of stimulation in excess of that seen for the wild-type receptor (data not shown). This suggests none of these substitution mutations forms a constitutively active receptor.

In contrast to the mutants described above, two constructs including a double alanine substitution of the valine and phenylalanine residues at positions 223 and 224 (V223A/F224A)CLR as well as a single mutation of tryptophan to alanine at position 232 (W232A)CLR, both resulted in a small loss in the ability of CLR to elevate cAMP in response to CGRP (Table 2 and Fig. 2, *b* and *c*). The disruption in signaling resulted in a significant reduction in the pEC$_{50}$ value of 4- and 2.6-fold for mutants (V223A/F224A)CLR and (W232A)CLR, respectively. However, when the His-216 or Lys-227 were mutated to alanine, the perturbation of cAMP was larger, with greater than an order of magnitude reduction in EC$_{50}$ (Table 2 and Fig. 2, *d* and *e*). This reduction corresponds to an 11- and 11.5-fold decrease for (H216A)CLR and (K227A)CLR, respectively. It is not without precedent that the effects of removing a basic residue such as Lys-227 are due to the destabilization of a salt bridge formed by an adjacent cationic side chain left without an ionic partner (in this case Glu-226), disrupting stability. To investigate this possibility, we constructed and analyzed a double mutant, (E226A/K227A)CLR. The signaling profile of this mutant was not significantly different to the effects seen by the (K227A)CLR mutant alone (pEC$_{50}$ values for wild-type and (E226A/K227A)CLR were 8.79 ± 0.08 and 8.28 ± 0.09, respectively, $n = 3$). These data suggest a direct role for the basic lysine side chain in the activation mechanism of the receptor.

ELISA Analysis of Cell-surface Expression—The mutants with disrupted cAMP signaling were subsequently analyzed for their comparative ability to traffic to the cell surface using a whole-cell enzyme-linked immunosorbent assay to detect the surface expression of the engineered

representative of three to four similar experiments. Points are the mean $\pm$ S.E. of triplicate points. *a*, mutations with wild-type cAMP signaling; *b*, (V223A/F224A)CLR; *c*, (W232A)CLR; *d*, (H216A)CLR; *e*, (K227A)CLR.
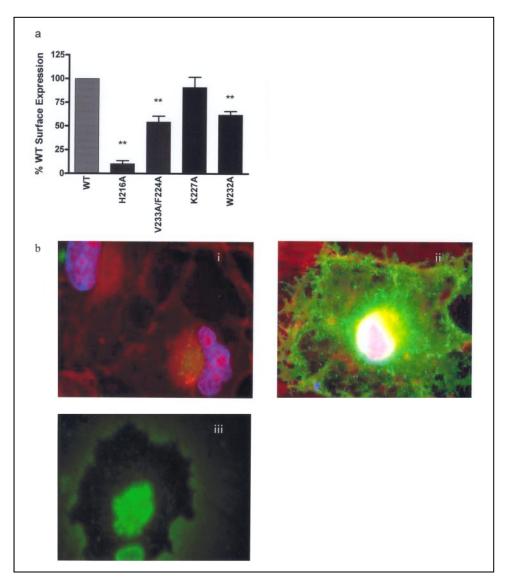
FIGURE 3. *a*, ELISA for H216A, V223A/F224A, K227A, and W232A. Surface expression of the four mutants with effects on adenylate cyclase activation is shown. **, significantly different from control; $p < 0.01$, 1-way analysis of variance followed by Dunnett's test. *b*, confocal microscopy. Cos-7 cells were transiently transfected with HA-tagged CLR and RAMP1. Cells were fixed, and immunohistocytochemistry was processed as shown under "Experimental Procedures." Images are representative from three separate experiments. *i*, cell transfected with RAMP1 alone; *ii*, cell transfected with HA-CL and RAMP1; *iii*, cell transfected with HA-CL alone.

HA-tag epitope. The ELISA data are shown graphically in Fig. 3*a*, and maximum absorbance values (AB_{max}) are summarized with their S.E. in Table 3. The alanine substitutions to the hydrophobic residues Val-223/Phe-224 and Trp-232 approximately halved cell-surface expression to 54.2 ± 6.2 and $61.8 \pm 3.8\%$ of wild type, respectively. (H216A)CLR was barely detected at the cell surface, with an expression level just $10.2 \pm 3.2\%$ of wild type. (K227A)CLR shows cell-surface expression levels comparable with wild type ($90.9 \pm 10.8\%$).

To validate that the ELISA analysis presents a valuable measure of cell surface expression, we investigated the cell surface localization of HA-tagged CLR using immunofluorescence confocal microscopy (Fig. 3*b*). As expected, no signal was visible in cells transfected with untagged RAMP1 alone (Fig. 3*b*, *i*). When HA-CLR was co-expressed with RAMP1, fluorescence was seen both inside the cell and on the plasma membrane (Fig. 3*b*, *ii*). In cells transfected with HA-CLR alone, little fluorescence was seen on the plasma membrane, although there was intense intracellular staining (Fig. 3*b*, *iii*). Although the microscopy experiments are a qualitative measure and cannot be a sound basis for estimates of total cellular expression, they confirmed the cell surface expression of these receptors, thus demonstrating the ELISA represents genuine surface expression.

TABLE 3
Expression and CGRP affinty of mutant receptors
Values are the mean ± S.E.; the number of determinations is shown in parentheses. B_{max} and K_d values determined from [^{125}I]-CGRP radioligand binding. AB_{max}; relative cell surface expression of receptors as measured by detection of HA tags in an ELISA. Data are normalized to WT as 100%.

Mutant	B_{max}	AB_{max}	K_d
	pmol/mg		*nM*
WT	1.60 ± 0.48 (12)	100 (3)	8.71 ± 0.07 (9)
H216A	1.45 ± 0.50 (3)	10.2 ± 3.2 (3)[a]	8.47 ± 0.09 (3)
V223A/F224A	2.91 ± 0.96 (3)	54.2 ± 6.2 (3)[a]	8.60 ± 0.19 (3)
K227A	1.62 ± 0.16 (3)	90.9 ± 10.8 (3)	9.16 ± 0.43 (3)
W232A	1.02 ± 0.36 (3)	61.8 ± 3.8 (3)[a]	8.62 ± 0.16 (3)

[a] Significantly different from WT; $p < 0.05$ compared to WT using one-way analysis of variance followed by Dunnett's test.

Radioligand Analysis of Total Cell Receptor Expression (B_{max})—The total cellular expression of transfected receptors was compared with wild type using radioligand binding analyses. Total expression (B_{max}) values were estimated from ^{125}I-labeled CGRP radioligand binding, calculating the amount bound by diluting the specific activity of the tracer radioligand with unlabeled CGRP. There was no significant difference between B_{max} values for any of the mutants and control (Table 3), showing that the reduced surface expression seen for (V223A/F224A)CLR,

[W232]CLR, and (H216A)CLR was reflective of a reduced localization or surface stability and not reduced protein expression or gross misfolding of the receptor.

CGRP Affinity-measured Using Radioligand Displacement Studies— In contrast to the reduced signaling efficacy of the above four mutants, CGRP-affinity measured using ^{125}I-labeled CGRP radioligand binding experiments was unaffected. Binding curves are shown in Fig. 4 with pK_d values presented in Table 3. This supports the suggestion that the effects seen by (H216A)CLR, (V223A/F224A)CLR, and [W232]CLR are not indirect effects on agonist binding. Interestingly, the wild-type affinity shown by (K227A)CLR suggests an effect on the activation mechanism of the CGRP receptor that is structurally downstream of conformational switch from ground state (*R*) to the high affinity activated state (*R**). The affinity of CGRP to the ground
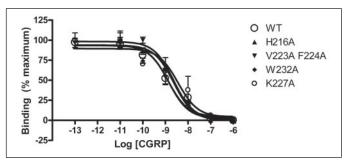

FIGURE 4. **Displacement of ^{125}I-labeled CGRP by unlabeled CGRP at the four functionally important mutants compared with WT.** Cos-7 cells were transfected with WT/RAMP1 or mutant/RAMP1, and membranes were assayed for ^{125}I-labeled CGRP binding. *Open circles*, WT type receptors. Mutant receptors are as indicated. Data are representative of three to four similar experiments. Points are the mean ± S.E. of triplicate points.
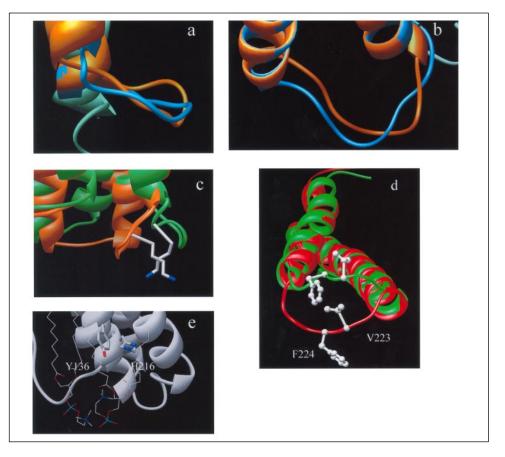
state of CLR/RAMP1 heterodimer has previously been shown to be reduced (7).

*Loop Modeling—*To further understand the effects of (K227A)CLR and (H216A)CLR, we set about to construct models of ICL2 in the probable inactive and active conformations of CLR. To assess the effectiveness of a loop modeling protocol, it must first be able to predict the conformation of loops from a protein whose structure has been solved to high resolution. Rhodopsin is the only GPCR whose structure is known in atomic detail, and as such, we have used the protocol of de Bakker *et al.* (29) to predict the conformation of ICL2.

The ICL2 of bovine rhodopsin is defined by the sequence ^{140}CKPM-SNFRFG^{149}, where C^{140} and G^{149} represent the intracellular ends of TM3 and TM4, respectively. Fig. 5, *a* and *b*, show the backbone conformation of the native structure, and superimposed on this is the highest-scored predicted conformation of ICL2 that was selected from an initial ensemble of 1000 random conformations. It is clear that the use of the AMBER/GBSA energy function resulted with the selection of a conformation with a fold that was very close to the native loop. Structural deviation between the native and predicted conformation of ICL2 was measured, which resulted with a heavy atom root mean-squared deviation of less than 1.0 Å.

*The Predicted Structure of ICL2 of CLR—*It is reasonable to assume that the conformation of the framework on which the loops are predicted would have an impact on the final loop orientation. With this in mind we have performed the same method as discussed above for bovine rhodopsin, on ICL2 from the CL receptor under two different starting conditions to explore the effects of conformational change on the orientation of the loop. The conditions for the loop predictions were 1) homology modeling and MD refinement based on the ground state x-ray crystal structure coordinates of bovine rhodopsin and 2) molecu-

FIGURE 5. **Loop modeling of ICL2 from bovine rhodopsin and CLR.** *a* and *b*, the backbone conformation of the highest scored loop prediction of rhodopsin ICL2 from the side and top, respectively (conformation of the x-ray crystal structure *orange*, best scored prediction *blue*). Whereas the complete TM bundle was used for the prediction of ICL2 only, TM3 and TM4 are shown for clarity. A backbone atom root mean-squared deviation was calculated between the native and predicted loop conformations and resulted in less than a 1-Å difference. *c*, ICL2 of the CLR in the inactive (*red*) and proposed active states (*green*) showing how lysine 227 changes orientation. *d*, ICL2 of the CLR in the inactive (*red*) and proposed active states showing how the side chains of valine 223 and phenylalanine 224 maintain their orientation with respect to each other despite their translocation. *e*, comparison of the position of histidine 216 in CLR with tyrosine 136 of bovine rhodopsin.

lar modeling, which utilized a refined TM helical bundle based experimentally derived distance constraints, which are consistent with an active conformation of bovine rhodopsin.

Comparison of the loop predictions for each of the starting conditions revealed distinct loop conformations for the inactive and a proposed active state of the receptor (Fig. 5*c*). It is clear that in the predicted inactive conformation, ICL2, acts to occlude the intracellular portion of the receptor. In contrast, the proposed active state revealed a conformational change that would allow access of G-proteins with the intracellular portion of the receptor. This is in contrast to the x-ray crystal structure of bovine rhodopsin where ICL2 does not act as a steric constraint in the inactive state of the receptor. However, several molecular dynamic studies (30) have demonstrated an increased root mean-squared fluctuation of the intracellular loops compared with the remainder of the protein, which is consistent with the *B*-factors found in the structural Protein Data Bank file. This suggests that ICL2 is dynamic and may adopt other conformations that are not observed in the rhodopsin x-ray crystal structures. In the model, the residues that alter cAMP production all undergo distinct conformational changes. The side chain of Lys-227 moves so that it is orientated toward the putative G-protein binding pocket in the active state of the receptor (Fig. 5*c*). Val-233 and Phe-234 undergo significant translations, but the relative orientations of their side chains relative to each in the active and inactive other remain constant; no other pair of side chains in ICL2 shows this property (Fig. 5*d*). His-216 shows virtually no change in position; it is located between a cavity between TMs 3, 4, and 5 and is lipid-facing (Fig. 5*e*). However, it is in a very similar position to Tyr-136 of bovine rhodopsin, part of the DRY motif of that receptor.

DISCUSSION

Defining the precise molecular roles of residues within the intracellular loops of G-protein-coupled receptors is of fundamental importance. These loops are the key to dissecting many aspects of pharmacological specificity, and individual residues within ICL2 have been shown to distinguish between different α-subunits of the G-protein complex (9). There are few functional studies published for the analysis of the transmembrane helix 3 proximal region of ICL2 for the family B receptors, although recent observations have suggested an involvement and possible movement of the bottom of TMs 3 and 6 in the activation of glucagon-like peptide 1 and CL receptors (7, 31), in line with current models of activation for the family A.

Unlike family A, there is no crystal structure of a family B GPCR to use for modeling studies. This is a particular problem in the region of transmembrane helix 3 for CLR, where two different proposals for the loop-helix boundary have been published (10, 32). Our re-evaluation of the likely TM-loop boundary suggests that the prediction of Chang *et al.* (32) is closest to the likely structure. Having established the likely loop-helix boundaries for ICL2, we have been able to model this region. The data suggest that movement of ICL2 is likely to play a significant role in CLR activation by exposing a binding pocket for G-proteins. This prediction is consistent with our findings from the mutagenesis which demonstrate that residues in the loop are implicated in activation of adenylyl cyclase.

Alanine-scanning mutagenesis of the entire second intracellular loop of CLR highlighted four residues or sets of residues that are important for signaling via cAMP. (V223A/F224A)CLR and (W232A)CLR showed small effects on surface expression and signaling. A previous study on the prostaglandin receptors suggested that a cluster of hydrophobic aromatic amino acids in ICL2 played a role in G_s coupling (33), and it is

possible that a similar factor is at work here. (K227A)CLR had a direct negative effect on cAMP signaling without disrupting surface expression. The wild-type agonist affinities of all these mutants imply that, although the residues are important for G-protein interaction (either directly or indirectly), they are not important in stabilizing the active conformation of the receptor around the CGRP binding state. The native uncoupled, ground state of the receptor has a significantly lower affinity for CGRP than the active form (7). The role for Lys-227 may involve downstream interaction with the G_s, although it may also be a candidate for receptor component protein interaction, which is thought to involve an ionic combination centered around the second intracellular loop of CLR (13). An effect specific for CL is consistent with the observation that interactions between the second intracellular loop and the $G\alpha_s$ subunit have been specifically dismissed for other members of both family B (9) and family A GPCRs (34). A lysine in a similar position in the family B parathyroid hormone receptor was shown to be required for signal transduction (albeit G_q- and not G_s-coupled) (9). The modeling suggests a mechanism for the effects of Lys-227, with the side chain pointed into a newly created cavity. It would now be able to interact with any G-protein that occupied the pocket. Interestingly, visual inspection of the active and inactive conformations of ICL2 reveal that Lys-227 is the only residue to be orientated closer to the G-protein binding pocket in the active state than in the inactive state (Fig. 5*c*). Furthermore, the side-chain length and charged state of Lys may make it able to form directive interactions at longer distances, as compared with other charged residues located in the ICL2. The modeling also sheds light on the roles of Val-233 and Phe-234. The unique preservation of the orientation of their side chains suggest that these residues may help maintain the loop integrity in this region of the receptor.

A surprising result was the identification of His-216 as important for cell-surface expression. The receptor can bind CGRP normally in cell homogenates, suggesting that the receptor folds correctly and associates with RAMPs but fails to be translocated to the cell surface. It may be part of a transport motif, or alternatively, it may act to mask an endoplasmic reticulum retention signal. The extreme C terminus of RAMP1 acts as an endoplasmic reticulum retention signal that must be overridden after association with CLR (35); His-216 may be involved in this process. The corresponding tyrosine to Tyr-214 in the glucagon-like peptide 1 receptor has been proposed to be the DRY-equivalent tyrosine residue in family B GPCRs (7, 31). Conversely, our data show that Tyr-214 has no functionally important role in the CGRP receptor, and therefore, this is not part of a family B motif conserved across the entire family. It is not out of the question that His-216, with a role in surface expression, may be the third member of a DRY equivalent. Histidine has been shown to be a natural replacement for the tyrosine residue of the DR(Y/H) motif of the family A V_2 vasopressin receptor (36). Interestingly, the V_2 receptor, like the CGRP receptor, signals predominantly through the $G\alpha_s$ subunit. Furthermore, this third member of the family A DR(Y/H) motif has been proposed in the m1 muscarinic receptor to form intramolecular contacts whose integrity is required for efficient receptor folding but does not necessarily participate directly in signaling (37). The similarity with the effects seen for His-216 in this study is striking. Furthermore, our modeling suggests that His-216 occupies a similar spatial position to Tyr-136 of the DRY motif in bovine rhodopsin.

In conclusion, this study shows that ICL2 of CLR plays an important part in coupling the receptor to cAMP production. Modeling suggests that the loop undergoes a significant change in conformation upon receptor activation. Lys-227 may directly interact with G_s. However, His-216 plays a separate role in ensuring cell-surface expression of the

receptor. It will be interesting to discover if ICL2 plays similar roles in other family B GPCRs.

REFERENCES

1. Palczewski, K., Kumasaka, T., Hori, T., Behnke, C. A., Motoshima, H., Fox, B. A., Le Trong, I., Teller, D. C., Okada, T., Stenkamp, R. E., Yamamoto, M., and Miyano, M. (2000) *Science* **289,** 739–745
2. Gershengorn, M. C., and Osman, R. (2001) *Endocrinology* **142,** 2–10
3. Kalatskaya, I., Schussler, S., Blaukat, A., Muller-Esterl, W., Jochum, M., Proud, D., and Faussner, A. (2004) *J. Biol. Chem.* **279,** 31268–31276
4. Urizar, E., Claeysen, S., Deupi, X., Govaerts, C., Costagliola, S., Vassart, G., and Pardo, L. (2005) *J. Biol. Chem.* **280,** 17135–17141
5. Erlenbach, I., Kostenis, E., Schmidt, C., Serradeil-Le Gal, C., Raufaste, D., Dumont, M. E., Pausch, M. H., and Wess, J. (2001) *J. Biol. Chem.* **276,** 29382–29392
6. Sheikh, S. P., Vilardarga, J. P., Baranski, T. J., Lichtarge, O., Iiri, T., Meng, E. C., Nissenson, R. A., and Bourne, H. R. (1999) *J. Biol. Chem.* **274,** 17033–17041
7. Conner, A. C., Hay, D. L., Simms, J., Howitt, S. G., Schindler, M., Smith, D. M., Wheatley, M., and Poyner, D. R. (2005) *Mol. Pharmacol.* **67,** 20–31
8. Couvineau, A., Lacapere, J. J., Tan, Y. V., Rouyer-Fessard, C., Nicole, P., and Laburthe, M. (2003) *J. Biol. Chem.* **278,** 24759–24766
9. Iida-Klein, A., Guo, J., Takemura, M., Drake, M. T., Potts, J. T., Jr., Abou-Samra, A., Bringhurst, F. R., and Segre, G. V. (1997) *J. Biol. Chem.* **272,** 6882–6889
10. Aiyar, N., Rand, K., Elshourbagy, N. A., Zeng, Z., Adamou, J. E., Bergsma, D. J., and Li, Y. (1996) *J. Biol. Chem.* **271,** 11325–11329
11. Conner, A. C., Simms, J., Hay, D. L., Mahmoud, K., Howitt, S. G., Wheatley, M., and Poyner, D. R. (2004) *Biochem. Soc. Trans.* **32,** 843–846
12. Evans, B. N., Rosenblatt, M. I., Mnayer, L. O., Oliver, K. R., and Dickerson, I. M. (2000) *J. Biol. Chem.* **275,** 31438–31443
13. Loiseau, S. C., and Dickerson, I. M. (2004) *Neuropeptides* **38,** 6 (abstr.)
14. McLatchie, L. M., Fraser, N. J., Main, M. J., Wise, A., Brown, J., Thompson, N., Solari, R., Lee, M. G., and Foord, S. M. (1998) *Nature* **393,** 333–339
15. Koller, D., Born, W., Leuthauser, K., Fluhmann, B., McKinney, R. A., Fischer, J. A., and Muff, R. (2002) *FEBS Lett.* **531,** 464–468
16. Poyner, D. R., Andrew, D. P., Brown, D., Bose, C., and Hanley, M. R. (1992) *Br. J. Pharmacol.* **105,** 441–447
17. Krogh, A., Larsson, B., von Heijne, G., and Sonnhammer, E. L. (2001) *J. Mol. Biol.* **305,** 567–580
18. Tusnady, G. E., and Simon, I. (2001) *Bioinformatics* **17,** 849–850
19. Wilbur, W. J., and Lipman, D. J. (1983) *Proc. Natl. Acad. Sci. U. S. A.* **80,** 726–730
20. Lindahl, E., Hess, B., and Spoel, D. V. D. (2001) *J. Mol. Model.* **7,** 306–317
21. Dunham, T. D., and Farrens, D. L. (1999) *J. Biol. Chem.* **274,** 1683–1690
22. Struthers, M., Yu, H., Kono, M., and Oprian, D. D. (1999) *Biochemistry* **38,** 6597–6603
23. Gouldson, P. R., Kidley, N. J., Bywater, R. P., Psaroudakis, G., Brooks, H. D., Diaz, C., Shire, D., and Reynolds, C. A. (2004) *Proteins* **56,** 67–84
24. Altenbach, C., Cai, K., Klein-Seetharaman, J., Khorana, H. G., and Hubbell, W. L. (2001) *Biochemistry* **40,** 15483–15492
25. Altenbach, C., Klein-Seetharaman, J., Cai, K., Khorana, H. G., and Hubbell, W. L. (2001) *Biochemistry* **40,** 15493–15500
26. Bower, M. J., Cohen, F. E., and Dunbrack, R. L., Jr. (1997) *J. Mol. Biol.* **267,** 1268–1282
27. Samudrala, R., and Moult, J. (1998) *J. Mol. Biol.* **275,** 895–916
28. Pappu, R. V., Marshall, G. R., and Ponder, J. W. (1999) *Nat. Struct. Biol.* **6,** 50–55
29. de Bakker, P. I., DePristo, M. A., Burke, D. F., and Blundell, T. L. (2003) *Proteins* **51,** 21–40
30. Crozier, P. S., Stevens, M. J., Forrest, L. R., and Woolf, T. B. (2003) *J. Mol. Biol.* **333,** 493–514
31. Frimurer, T. M., and Bywater, R. P. (1999) *Proteins* **35,** 375–386
32. Chang, C. P., Pearse, R. V., Jr., O'Connell, S., and Rosenfeld, M. G. (1993) *Neuron* **11,** 1187–1195
33. Sugimoto, Y., Nakato, T., Kita, A., Takahashi, Y., Hatae, N., Tabata, H., Tanaka, S., and Ichikawa, A. (2004) *J. Biol. Chem.* **279,** 11016–11026
34. Kang, H., Lee, W. K., Choi, Y. H., Vukoti, K. M., Bang, W. G., and Yu, Y. G. (2005) *Biochem. Biophys. Res. Commun.* **329,** 684–692
35. Steiner, S., Muff, R., Gujer, R., Fischer, J. A., and Born, W. (2002) *Biochemistry* **41,** 11398–11404
36. Morin, D., Cotte, N., Balestre, M. N., Mouillac, B., Manning, M., Breton, C., and Barberis, C. (1998) *FEBS Lett.* **441,** 470–475
37. Lu, Z. L., Curtis, C. A., Jones, P. G., Pavia, J., and Hulme, E. C. (1997) *Mol. Pharmacol.* **51,** 234–241

The Second Intracellular Loop of the Calcitonin Gene-related Peptide Receptor Provides Molecular Determinants for Signal Transduction and Cell Surface Expression

Alex C. Conner, John Simms, Stephen G. Howitt, Mark Wheatley and David R. Poyner

Access the most updated version of this article at doi: 10.1074/jbc.M510064200

Alerts:
- When this article is cited
- When a correction for this article is posted

Click here to choose from all of JBC's e-mail alerts

This article cites 37 references, 14 of which can be accessed free at
http://www.jbc.org/content/281/3/1644.full.html#ref-list-1